NeuroImage 200 (2019) 302–312

Contents lists available at ScienceDirect

NeuroImage

journal homepage: www.elsevier.com/locate/neuroimage

Development of a transcallosal tractography template and its application to dementia

Derek B. Archer [a], Stephen A. Coombes [a], Nikolaus R. McFarland [b], Steven T. DeKosky [c], David E. Vaillancourt [a,b,d,*]

[a] Laboratory for Rehabilitation Neuroscience, Department of Applied Physiology and Kinesiology, University of Florida, Gainesville, FL, USA
[b] Department of Neurology and Fixel Center for Neurological Disease, College of Medicine, University of Florida, Gainesville, FL, USA
[c] Department of Neurology and McKnight Brain Institute, University of Florida, Gainesville, FL, USA
[d] Department of Biomedical Engineering, University of Florida, Gainesville, FL, USA

ARTICLE INFO

Keywords:
Corpus callosum
Alzheimer's disease
Progressive supranuclear palsy
Free-water
Template
Atlas

ABSTRACT

Understanding the architecture of transcallosal connections would allow for more specific assessments of neurodegeneration across many fields of neuroscience, neurology, and psychiatry. To map these connections, we conducted probabilistic tractography in 100 Human Connectome Project subjects in 32 cortical areas using novel post-processing algorithms to create a spatially precise Trancallosal Tract Template (TCATT). We found robust transcallosal tracts in all 32 regions, and a topographical analysis in the corpus callosum largely agreed with well-established subdivisions of the corpus callosum. We then obtained diffusion MRI data from a cohort of patients with Alzheimer's disease (AD) and another with progressive supranuclear palsy (PSP) and used a two-compartment model to calculate free-water corrected fractional anisotropy (FA_T) and free-water (FW) within the TCATT. These metrics were used to determine between-group differences and to determine which subset of tracts was best associated with cognitive function (Montreal Cognitive Assessment (MoCA)). In AD, we found robust between-group differences in FW (31/32 TCATT tracts) in the absence of between-group differences in FA_T. FW in the inferior temporal gyrus TCATT tract was most associated with MoCA scores in AD. In PSP, there were widespread differences in both FA_T and FW, and MoCA was predicted by FA_T in the inferior frontal pars triangularis, preSMA, and medial frontal gyrus TCATT tracts as well as FW in the inferior frontal pars opercularis TCATT tract. The TCATT improves spatial localization of corpus callosum measurements to enhance the evaluation of treatment effects, as well as the monitoring of brain microstructure in relation to cognitive dysfunction and disease progression. Here, we have shown its direct relevance in capturing between-group differences and associating it with the MoCA in AD and PSP.

1. Introduction

The corpus callosum is composed of approximately 200 million commissural fibers connecting the bilateral prefrontal, frontal, parietal, occipital, and temporal lobes (Tomasch, 1954). While this is well-known, a 3-dimensional representation with high resolution to adequately sample many tracts traversing the corpus callosum is not available. Understanding the architecture of these connections would allow for more specific assessments of structural deficits and structure-function relationships across many fields of neuroscience, neurology, and psychiatry. Further, it could allow for more enhanced measurements of disease progression, evaluation of treatment effects, and improve patient selection for clinical trials.

Diffusion MRI is a non-invasive method enabling the characterization of white matter tracts, and several impactful studies have conducted tractography of the transcallosal tracts (Abe et al., 2004; Arnone et al., 2008; Caeyenberghs et al., 2011; Hofer and Frahm, 2006; Huang et al., 2005; Lebel et al., 2010; Liu et al., 2010; Pannek et al., 2010). However, a comprehensive, high resolution tractography template has not been made freely available to the public. The present study incorporates several novel components to create a new, multi-tract, transcallosal tractography template. First, it characterizes the commissural

* Corresponding author. University of Florida, Laboratory for Rehabilitation Neuroscience, Department of Applied Physiology and Kinesiology, PO Box 118205, Gainesville, FL, 32611-8205, USA.
E-mail address: vcourt@ufl.edu (D.E. Vaillancourt).

https://doi.org/10.1016/j.neuroimage.2019.06.065
Received 20 March 2019; Received in revised form 12 June 2019; Accepted 27 June 2019
Available online 28 June 2019

connections of 32 different cortical regions, while a majority of prior studies have only parcellated 5–8 large-scale connections to the orbital, frontal, parietal, occipital, and temporal lobes (Arnone et al., 2008; Caeyenberghs et al., 2011; Hofer and Frahm, 2006; Huang et al., 2005; Lebel et al., 2010; Liu et al., 2010). Second, it utilizes a large cohort of 100 Human Connectome Project (HCP) subjects, the data from which has a higher resolution than conventional diffusion MRI (Van Essen et al., 2013). Third, this template is generated with a novel slice-level post--processing approach which minimizes false positive and false negative voxels in the resulting tract template (Archer et al., 2018b).

A transcallosal tractography template would be particularly useful in the assessment of different neurodegenerative dementias, such as Alzheimer's disease (AD) and progressive supranuclear palsy (PSP). Currently, diagnostic confirmation of these diseases requires the demonstration of specific post-mortem brain pathology or visualizing the defining abnormal protein aggregates on positron emission tomography or in CSF. *In-vivo* biomarkers that serve as proxies of neurodegeneration may be valuable indicators of initiation or progression of disease state (Jack et al., 2018). In AD, there is widespread commissural atrophy, while in PSP there is more focal and relatively preserved commissural structure. Many studies have used diffusion MRI in AD and PSP to evaluate commissural degeneration. In AD, fractional anisotropy (FA) is consistently reduced in the genu and splenium (Duan et al., 2006; Naggara et al., 2006; Ouyang et al., 2015; Takahashi et al., 2002; Teipel et al., 2007; Zhang et al., 2007). In PSP, FA is primarily reduced in the genu and body of the corpus callosum (Ito et al., 2008; Lehericy et al., 2010; Whitwell et al., 2011). Other studies, however, have found no significant differences between disease states and healthy controls (Choi et al., 2005; Duan et al., 2006; Head et al., 2004; Naggara et al., 2006; Takahashi et al., 2002; Zhang et al., 2007), which could be due to the susceptibility of FA to partial volume effects, as each voxel has both a tissue component and a fluid component. Free-water imaging has advanced diffusion MRI by allowing for the separation of these components within each voxel (Pasternak et al., 2009). Such an advance may aid definition of callosal microstructure if applied to large datasets of AD and PSP, thus enhancing the evaluation of transcallosal tract microstructure and its association with a measure of cognitive function (Nasreddine et al., 2005).

There are two goals in the current study. First, we have taken advantage of the recent advancements in tractography post-processing techniques to create a transcallosal tract template consisting of 32 different tracts using a cohort of 100 HCP subjects using regions from the automated anatomical labeling parcellation (Tzourio-Mazoyer et al.,

Table 1
Subject demographics and relevant clinical information.

Measure	AD Cohort			PSP Cohort		
	AD	Control	Statistics	PSP	Control	Statistics
N	30	32	–	26	31	–
Sex	(17M/13F)	(12M/20F)	$\chi2 = 2.285$; $p = 0.203$	(15M/11F)	(12M/19F)	$\chi2 = 0.076$; $p = 0.783$
Age (years)	73.99 (8.37)	72.73 (5.98)	$F = 3.774$; $p = 0.494$	69.88 (6.38)	63.23 (10.08)	$F = 7.57$; $p = 0.004$
MoCA	17.72 (4.66)	26.06 (2.45)	$F = 7.793$; $p < 0.001$	20.23 (5.33)	26.96 (1.92)	$F = 35.151$; $p < 0.001$

Data are either count or mean (±SD). Abbreviations: AD, Alzheimer's disease; PSP, Progressive Supranuclear Palsy; N, Number; M, Male; F, Female; MoCA, Montreal Cognitive Assessment.

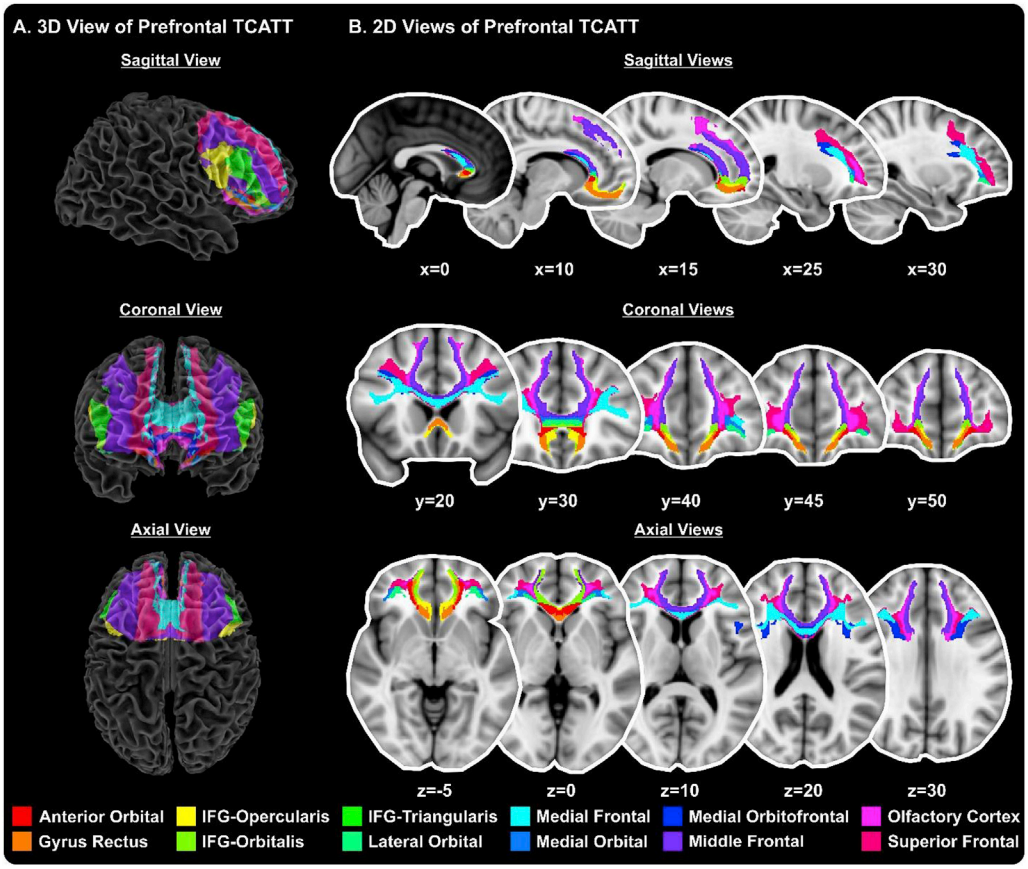

Fig. 1. The Transcallosal Tract Template (TCATT) Prefrontal Tracts. The TCATT contains 3-dimensional commissural connections of 12 different prefrontal cortical areas (**A**), including the anterior orbital gyrus, gyrus rectus, inferior frontal gyrus pars opercularis (IFG-Opercularis), inferior frontal gyrus pars orbitalis (IFG-Orbitalis), inferior frontal gyrus pars triangularis (IFG-Triangularis), lateral orbital gyrus, medial frontal gyrus, medial orbital gyrus, medial orbitofrontal gyrus, middle frontal gyrus, olfactory cortex, and the superior frontal gyrus. (**B**) The 2-dimensional representation of these tracts in the sagittal view ($x = 0, 10, 15, 25, 30$), coronal view ($y = 20, 30, 40, 45, 50$), and axial view ($z = -5$, $z = 0$, $z = 10$, $z = 20$, $z = 30$).

2002; Van Essen et al., 2013). Because it has been technically difficult to separate neighboring tracts in structural imaging, we utilized a novel post-processing technique which allows for their segmentation (Archer et al., 2018b). As this template was created in the MNI space, it allowed us to easily apply it to new datasets which were also in the MNI space. We therefore obtained a dataset from a well-defined multisite AD cohort from the Alzheimer's Disease Neuroimaging Initiative (ADNI), and a separate PSP cohort from the University of Florida. Since these cohorts were acquired from different MRI scanners, there are no direct comparisons between AD and PSP, but direct comparisons were made to respective control groups. We then used the transcallosal tractography template to evaluate microstructure deficits in each cohort and determined its association with general cognitive function.

2. Methods

2.1. HCP cohort

Diffusion MRI data from 100 healthy young individuals (54 females, 46 males; ages 21–35 were obtained from the HCP website (http://www.humanconnectomeproject.org) (Feinberg et al., 2010; Moeller et al., 2010; Setsompop et al., 2012; Sotiropoulos et al., 2013b; Van Essen et al., 2013). Diffusion images (resolution: 1.25 mm x 1.25 mm x 1.25 mm isotropic; slices: 111; FOV: 210 × 180; flip angle: 78°; b-values: 1000, 2000, and 3000 s/mm^2; number of directions per shell: 90; TE: 89.5 ms; TR: 5520 ms; number of b0s: 18; multiband factor: 3) were collected via a customized Siemens 3T scanner ("Connectome Skyra") (Sotiropoulos et al., 2013a; Van Essen et al., 2013). The HCP data were eddy current corrected and motion corrected prior to download. Following download, BEDPOSTx was conducted to fit fiber distributions at the voxel level to prepare for tractography analysis in FSL (i.e., probtrackx2). Moreover, DTIFIT was conducted for all HCP subjects to obtain fractional anisotropy maps. For all analyses, the grad_dev.nii.gz, a file available through the HCP website for each subject, was used to correct for gradient nonlinearities on the bvals and bvecs at the voxel level. Nonlinear warps which were provided by the HCP were used to transform all maps into the MNI space (Andersson and Sotiropoulos, 2016; Archer et al., 2018b; Jenkinson et al., 2012). The HCP cohort was used to develop the tractography template.

2.2. Alzheimer's disease (AD) and progressive supranuclear palsy (PSP) cohorts

2.2.1. Data acquisition

The present study included 2 separate disease cohort datasets – an AD cohort obtained from the ADNI database (imaging parameters – TR: ~11,000 ms, TE: 67 ms, flip angle: 90°, field of view: 350 × 350 mm, resolution: 2.7 mm isotropic, 41 non-collinear diffusion directions, b-value of 1000 s/mm^2 and five with b-values of 0 s/mm^2, 59 axial slices) and a PSP cohort obtained from the University of Florida (UF) (imaging parameters – TR: 7748 ms, TE: 86 ms, flip angle: 90°, field of view: 224 × 224 mm, resolution: 2 mm isotropic, 64 non-collinear diffusion directions, b-value of 1000 s/mm^2 and one with a b-value of 0 s/mm^2, 75 axial slices). The AD cohort included 62 participants: 30 with AD and 32 cognitively normal controls. The PSP cohort included 57 participants: 26 with PSP and 31 cognitively normal controls. Cognitive function of all participants was measured using the Montreal Cognitive Assessment (MoCA) (Nasreddine et al., 2005). The AD cohort data were acquired from 10 different scanners, while PSP cohort data were acquired from 1 scanner. For this reason, scanner site was included as a covariate in all AD cohort analyses. In all analyses, we compared the AD and PSP cohorts

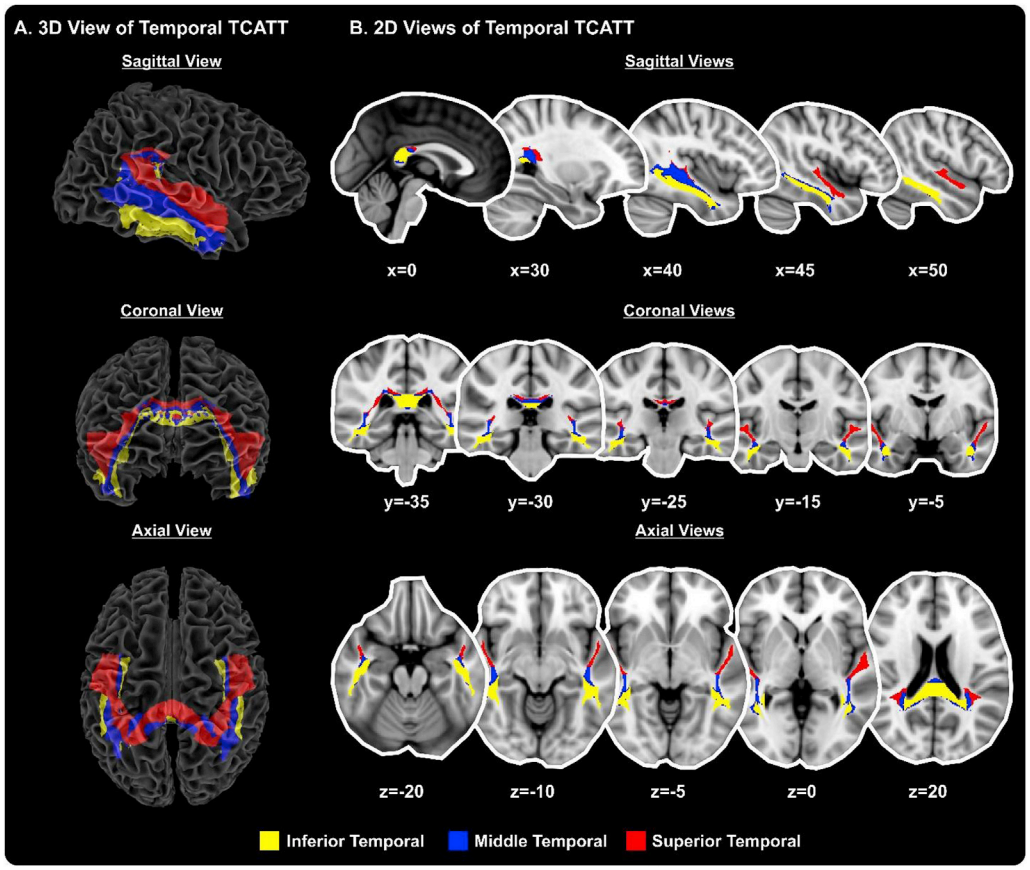

Fig. 2. The Transcallosal Tract Template (TCATT) Temporal Tracts. The TCATT contains 3-dimensional commissural connections of 3 different temporal cortical areas (**A**), including the inferior temporal gyrus, middle temporal gyrus, and superior temporal gyrus. (**B**) The 2-dimensional representation of these tracts in the sagittal view (x = 0, 30, 40, 45, 50), coronal view (y = −35, −30, −25, −15, −5), and axial view (z = −20, z = −10, z = −5, z = 0, z = 20).

separately to their respective control groups. Sex, age, and MoCA scores can all be found in Table 1.

2.2.2. Data preprocessing

FSL (fsl.fmrib.ox.ac.uk) was used for all diffusion MRI data analyses (Jenkinson et al., 2012; Smith et al., 2004; Woolrich et al., 2009). The data for all subjects was first corrected for eddy currents, then for head motion using a 3D affine registration, after which the brain data were extracted (Smith, 2002). The b vectors file was rotated to correspond to these changes in orientation. The motion and eddy current-corrected volume was then used to calculate free-water (FW) maps (i.e., the fluid component map) and free-water corrected fractional anisotropy (FA_T) maps (i.e., the tissue component map) using custom written MATLAB code (R2013a, The Mathworks, Natick, MA, USA), which was consistent with prior work (Archer et al., 2018a; Ofori et al., 2015; Pasternak et al., 2009). To obtain a standardized space representation of the FW and FA_T maps, each image was registered to its respective in-house template in standard space (1 mm isotropic) by a nonlinear warp using the Advanced Normalization Tools (ANTs) (Avants et al., 2008). Specifically, we used the SyNCC option in ANTs, which applies both an affine and deformation transformation to the FA and FA_T maps using cross correlation as the optimization metric.

2.3. Creation of the transcallosal tract template (TCATT)

Tractography analyses were conducted to map the transcallosal white matter pathways. Well-established atlases were utilized for inputs to generate tracts from distinct cortical areas (Desikan et al., 2006; Mayka et al., 2006). Probabilistic tractography was conducted using the probtrackx2 program in FSL using default settings (samples: 5000; curvature threshold: 0.2; FA threshold: 0.2) (Behrens et al., 2003, 2007) on all individuals in the HCP cohort. Tractography was conducted using the corpus callosum as a seed, with the 32 different cortical areas in the left and right hemispheres as target masks, including the inferior temporal gyrus, middle temporal gyrus, superior temporal gyrus, lingual gyrus, calcarine sulcus, cuneus, inferior occipital gyrus, middle occipital gyrus, superior occipital gyrus, angular gyrus, inferior parietal lobule, supramarginal gyrus, superior parietal lobule, paracentral lobule, somatosensory cortex, primary motor cortex, dorsal premotor cortex, ventral premotor cortex, pre-supplementary motor area, supplementary motor area, inferior frontal gyrus pars opercularis, medial frontal gyrus, middle frontal gyrus, inferior frontal gyrus pars triangularis, inferior frontal gyrus pars orbitalis, lateral orbital gyrus, superior frontal gyrus, anterior orbital gyrus, gyrus rectus, medial orbital gyrus, medial orbitofrontal gyrus, and olfactory cortex. Since tractography was conducted in both hemispheres separately, the results from the right hemisphere were flipped and averaged with the left hemisphere results. This averaged image was then averaged across all 100 HCP individuals for each tract. This group image was then thresholded at 15% maximum using a slice-level thresholding approach which allows for delineation of neighboring tracts without sacrificing volume in lowly probable portions of the tract (Archer et al., 2018b). This thresholded tract was flipped back to the right hemisphere to produce an identical bilateral tract for each cortical area. Slice-level thresholding was conducted along the primary axis of travel for each tract.

2.4. TCATT evaluation in AD and PSP

FA_T and FW differences in the TCATT were calculated by conducting false discovery rate (FDR) corrected independent samples t-tests. For each *t*-test, we tested the homogeneity of group variances by conducting a Levene's test. Depending on results of the Levene's test, a parametric (independent samples *t*-test) or a non-parametric (Mann-Whitney *U* test) analysis was conducted. Significance level was set at $p_{FDR}<0.05$. In total,

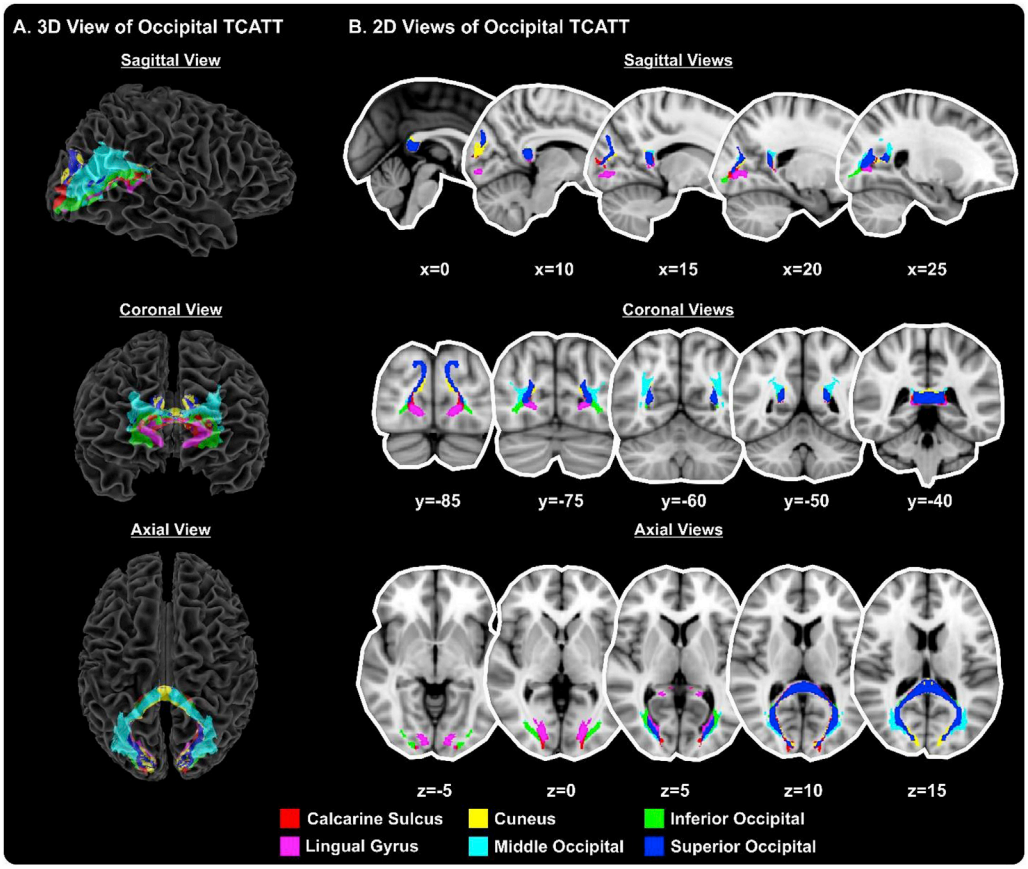

Fig. 3. The Transcallosal Tract Template (TCATT) Occipital Tracts. The TCATT contains 3-dimensional commissural connections of 6 different occipital cortical areas (**A**), including the calcarine sulcus, cuneus, inferior occipital gyrus, lingual gyrus, middle occipital gyrus, and superior occipital gyrus. (**B**) The 2-dimensional representation of these tracts in the sagittal view (x = 0, 10, 15, 20, 25), coronal view (y = −85, −75, −60, −50, −40), and axial view (z = −5, z = 0, z = 5, z = 10, z = 15).

32 t-tests (one *t*-test for each tract) were conducted for FA_T and FW for each cohort. Significant tract-wide differences were followed with slice-level between-group t-tests to determine region specific differences of FA_T and FW in each tract. A custom Linux shell-script computed the average FA_T and FW at each slice along the primary axis of travel for each tract. The average FA_T and FW was then compared separately between patients and controls, for each tract in each cohort, by conducting FDR-corrected independent samples t-tests.

2.5. Associating TCATT microstructure with cognitive function using stepwise multiple regression in AD and PSP

Significant slice-level results were used as independent variables in bidirectional stepwise multiple regression analyses to determine which measures were best associated with the MoCA. The model which resulted in the lowest Bayesian information criterion (BIC) was selected as the best fit model. Multicollinearity in the resulting models was quantified using the variance inflation factor (VIF); variables with VIF > 10 were removed. Stepwise multiple regression analyses were conducted separately in the AD and PSP cohorts. Control subjects were included in their respective cohort analyses. Significant neuroimaging variables and behavioral variables (AD cohort: age/gender/site; PSP cohort: age/gender) were included as independent variables.

3. Results

3.1. Transcallosal tract template (TCATT)

The TCATT includes the 3-dimensional commissural connections of 12 prefrontal cortical areas (Fig. 1A), which includes the anterior orbital gyrus, gyrus rectus, inferior frontal gyrus pars opercularis, inferior frontal gyrus pars orbitalis, inferior frontal gyrus pars triangularis, lateral orbital gyrus, medial frontal gyrus, medial orbital gyrus, medial orbitofrontal gyrus, middle frontal gyrus, olfactory cortex, and superior frontal gyrus. The segregation of these tracts can be seen in the sagittal, coronal, and axial views (Fig. 1B). The TCATT also includes 3 different temporal commissural tracts (Fig. 2), including the inferior temporal gyrus, middle temporal gyrus, and superior temporal gyrus. In addition to 12 prefrontal and 3 temporal commissural tracts, the TCATT includes 6 occipital (Fig. 3), 5 parietal (Fig. 4), and 6 frontal (Fig. 5) commissural tracts.

3.2. TCATT corpus callosum topography in young normal subjects

Corpus callosum population maps were averaged across the 100 HCP subjects (Fig. 6). Maps were thresholded at 15% so that only voxels which had at least 15% of the maximum number of streamlines were included in the population maps. The occipital topography maps (Fig. 6A) illustrate that a majority of the streamlines traversed through the most inferior portion of the splenium, with brighter colors indicating a higher probability of being a part of the tract of interest. Topographical maps were also created for the parietal, temporal, frontal, and prefrontal commissural tracts (Fig. 6B–E).

3.3. TCATT evaluation in AD

FA_T and FW within each of the 32 tracts was quantified in the AD cohort (means, standard deviations, and FDR corrected p values for each tract and each measure in Supplemental Table I) and FDR corrected t-

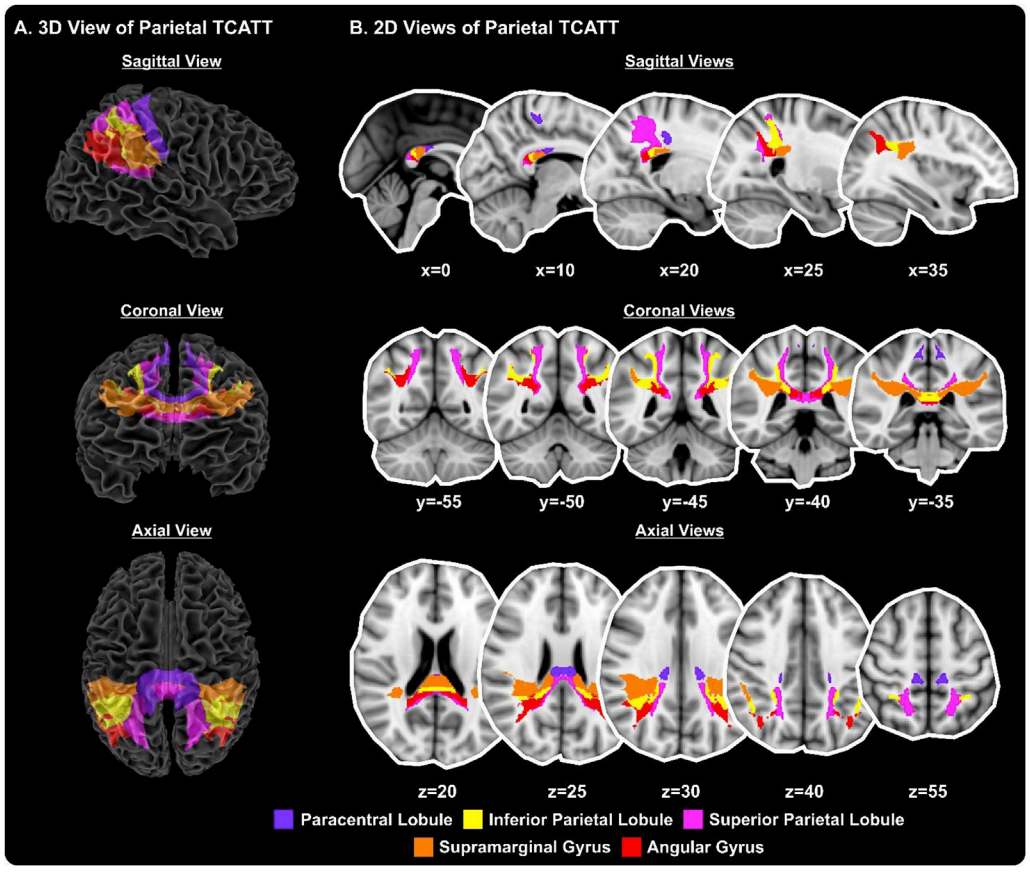

Fig. 4. The Transcallosal Tract Template (TCATT) Parietal Tracts. The TCATT contains 3-dimensional commissural connections of 5 different parietal cortical areas (**A**), including the paracentral lobule, inferior parietal lobule, superior parietal lobule, supramarginal gyrus, and angular gyrus. (**B**) The 2-dimensional representation of these tracts in the sagittal view (x = 0, 10, 20, 25, 35), coronal view (y = −55, −50, −45, −40, −35), and axial view (z = 20, z = 25, z = 30, z = 40, z = 55).

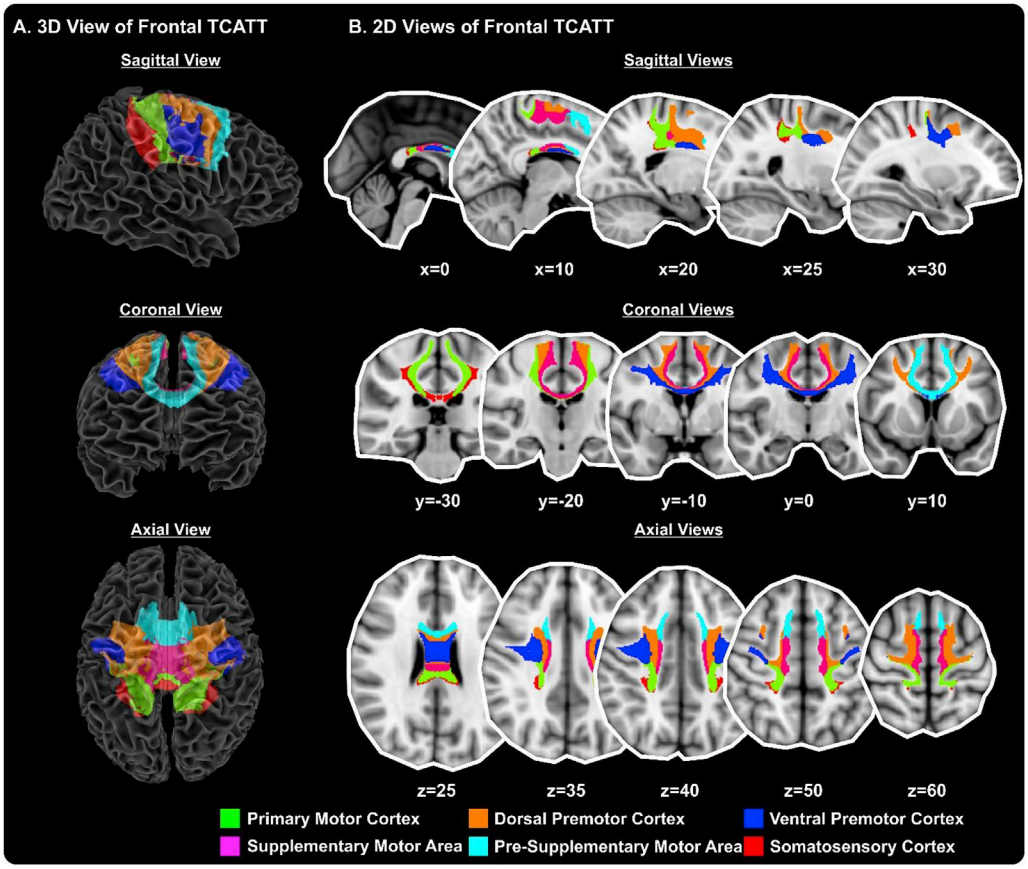

Fig. 5. The Transcallosal Tract Template (TCATT) Frontal Tracts. The TCATT contains 3-dimensional commissural connections of 6 different frontal cortical areas (**A**), including the primary motor cortex, dorsal premotor cortex, ventral premotor cortex, supplementary motor area, pre-supplementary motor area, and somatosensory cortex. (**B**) The 2-dimensional representation of these tracts in the sagittal view ($x = 0$, 10, 20, 25, 30), coronal view ($y = -30$, -20, -10, 0, 10), and axial view ($z = 25$, $z = 35$, $z = 40$, $z = 50$, $z = 60$).

tests were conducted to determine between-group differences for each measure. Following FDR correction, there were no significant between-group differences in FA_T (blue, Fig. 7A). In contrast, there were widespread between-group differences in FW (pink, Fig. 7B).

Tracts which demonstrated significant between-group differences underwent a slice-level analysis which determined the average FA_T and FW within each slice along the primary axis of travel. Slices which survived FDR corrected t-tests for each tract are provided (Supplemental Table I). Further, we provide an illustration of this analysis for the inferior temporal gyrus TCATT (Fig. 7C). The inferior temporal gyrus TCATT extended from $z = -36$ to $z = 25$. In Fig. 7C, mean difference between FA_T in AD and controls is shown with a blue line, and FW is shown with a pink line. All slices exhibited significantly increased FW in AD compared to controls. Following slice-level analysis, all significant slices for each tract were averaged and inputted into a bidirectional stepwise regression analysis, which minimized the Bayesian information criterion. A significant model was produced ($R^2_{adj} = 46.97\%$; $p < 0.001$), which included FW for the inferior temporal gyrus TCATT and scanner site, and a predicted vs. actual plot for MoCA showed good agreement (Fig. 7D).

3.4. TCATT evaluation in PSP

FA_T and FW within each of the 32 tracts was quantified in the PSP cohort (means, standard deviations, and FDR corrected p values for each tract and each measure in Supplemental Table II) and FDR corrected t-tests were conducted to determine between-group differences for each measure. Following FDR correction, a significant number of tracts exhibited reductions in FA_T and increases in FW in PSP compared to controls (Fig. 8A–B).

Tracts which demonstrated significant between-group differences underwent a slice-level analysis which determined the average FA_T and FW within each slice along the primary axis of travel. Slices which survived FDR corrected t-tests for each tract are provided (Supplemental Table II). Further, we provide an illustration of this analysis for the ventral premotor cortex TCATT (Fig. 8C). The ventral premotor cortex TCATT extended from $x = -50$ to $x = 50$. In Fig. 8C, mean difference in FA_T between PSP and controls is shown with a blue line, and FW is shown with a pink line. For both FA_T and FW, a majority of the tract demonstrated significant between-group differences. Following slice-level analysis, all significant slices for each tract and each measure were averaged and inputted into a bidirectional stepwise regression analysis, which minimized the Bayesian information criterion. A significant model was produced ($R^2_{adj} = 59.40\%$; $p < 0.001$), which included gender, FA_T in the inferior frontal pars triangularis, preSMA, and medial frontal gyrus commissural TCATT tracts as well as and FW in the inferior frontal pars opercularis commissural TCATT tract, and a predicted vs. actual plot for MoCA showed good agreement (Fig. 8D).

4. Discussion

This study created a high-resolution template of the transcallosal white matter tracts in normal subjects, and applied this template to compare cohorts of age-equivalent normal subjects with patients with Alzheimer's disease (AD) and progressive supranuclear palsy (PSP). To accomplish our first goal, we conducted probabilistic tractography in a large cohort of 100 HCP subjects in conjunction with a novel slice-level thresholding approach which allows for the segmentation of neighboring tracts (Archer et al., 2018b), which allowed us to identify 32 transcallosal tracts (12 prefrontal, 6 frontal, 5 parietal, 6 occipital, and 3 temporal tracts) and establish the transcallosal tract template (TCATT). The TCATT is now publicly available at www.lrnlab.org. Our second goal was to determine if free-water imaging was capable of identifying between-group differences and if FW and FA_T content was associated

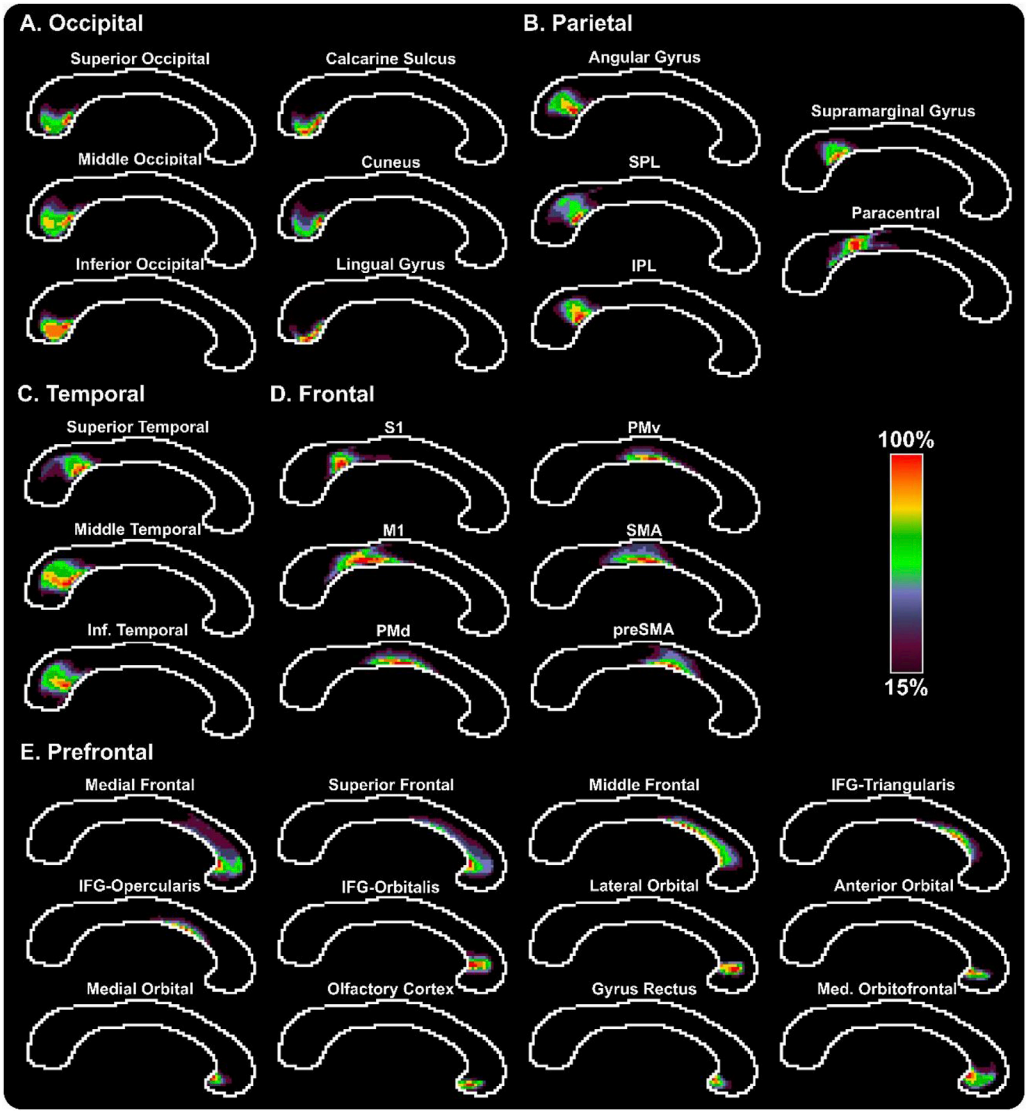

Fig. 6. TCATT Topography in the Corpus Callosum in Young Healthy Adults. Probabilistic group maps are shown for each TCATT tract, grouped into their respective lobes (**A** – Occipital, **B** – Parietal, **C** – Temporal, **D** – Frontal, **E** – Prefrontal). The color bar ranges from purple (15%) to red (100%), with higher intensity indicating higher probability that a voxel is within a tract. Voxels with less than 15% probability have been excluded from the group maps. Abbreviations: IFG, inferior frontal gyrus; M1, primary motor cortex; PMd, dorsal premotor cortex; PMv, ventral premotor cortex; SMA, supplementary motor area; preSMA, pre-supplementary motor area; S1, somatosensory cortex; IPL, inferior parietal lobule; SPL, superior parietal lobule.

with cognitive function. We therefore obtained diffusion MRI images from an AD and matched control cohort (30 AD, 32 controls) and a similarly matched PSP cohort (26 PSP, 31 controls), and quantified FW and FA_T within each TCATT tract for each individual. Following calculation of the mean FA_T and FW within each tract, we found widespread increases in TCATT FW in the AD cohort in the absence of alterations in FA_T. In the PSP cohort, there were widespread reductions in TCATT FA_T but increases in FW. Further, TCATT microstructure was associated with cognitive function in both cohorts.

Several studies have conducted tractography of the transcallosal white matter tracts, but recent advancements in diffusion MRI have allowed for higher resolution, larger cohort sizes, and more advanced post-processing algorithms. Over the last 10 + years, studies which have conducted tractography of the transcallosal white matter tracts either focused on transcallosal connectivity to entire lobes (Arnone et al., 2008; Caeyenberghs et al., 2011; Hofer and Frahm, 2006; Huang et al., 2005; Lebel et al., 2010; Liu et al., 2010) or have focused on more precise connections within specific lobes (Abe et al., 2004; Fling et al., 2013), with a majority of studies focusing on the former.

While the aforementioned tractography studies have provided insight into the transcallosal connections, other studies have conducted more spatially precise analyses. Pannek et al. (2010) conducted probabilistic tractography in 8 healthy individuals with diffusion MRI of 2.5 mm isotropic resolution to map 33 distinct transcallosal tracts (Pannek et al., 2010). They provided group averaged corpus callosum population maps to give the most spatially precise corpus callosum topographical map to date. Our current study advances the approach by Pannek et al. (2010) in three key ways. First, the diffusion MRI images of 1.25 mm isotropic resolution obtained from the HCP provided an 1/8 reduction in voxel volume, which allowed for the modelling of three fibers per voxel and therefore provided a more accurate assessment of crossing fibers. Second, using a cohort of 100 individuals and creating group-averaged tract templates, we were able to reduce spatial variability. Third, we implemented a slice-level thresholding approach to probabilistic tractography output, enabling minimization of both false negative and false positive voxels in the templates (Archer et al., 2018b). Importantly, our TCATT results largely agree with the Hofer and Frahm segmentation of the corpus callosum (Hofer and Frahm, 2006). While the Hofer and Frahm segmentation is a well-known baseline for corpus callosum topography, advances in tractography have allowed for more specificity. A recent study used constrained spherical deconvolution in 130 healthy subjects to find distinct organization of several prefrontal tracts, including the superior frontal gyrus, middle frontal gyrus, and inferior frontal gyrus (De Benedictis et al., 2016). They found that homotopic connections of the superior frontal gyrus were located in a dorso-medial portion of the anterior corpus callosum, while the middle frontal gyrus and inferior

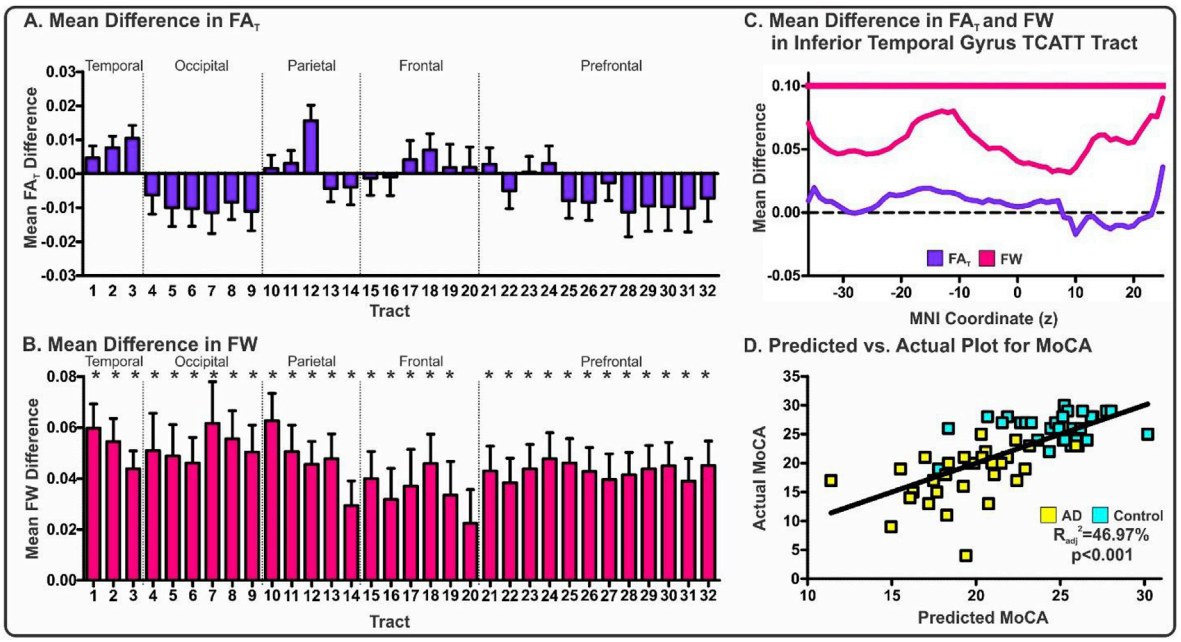

Fig. 7. Evaluation of FA_T and FW within the TCATT for the AD Cohort. Mean differences in FA_T (**A**) and FW (**B**) for AD-control for each TCATT tract grouped by their cortical projection (Temporal, Occipital, Parietal, Frontal, Prefrontal). Columns represent mean difference between group and error bars represent standard deviation. Significant mean differences were followed with slice-level analyses. The FA_T (blue) and FW (pink) profiles for the inferior temporal gyrus commissural TCATT tract are shown in (**C**), where FDR corrected t-tests were performed at each slice, in which age, sex, and scanner site were inputted as covariates. Slices which exhibited FDR corrected significance ($p_{FDR}<0.05$) are shown with horizontal blue or pink lines. (**D**) The predicted versus actual plot for the input variables which were most associated with MoCA in the AD cohort (AD: yellow; Control: cyan), which included FW in inferior temporal gyrus TCATT tract and scanner site. Abbreviations: 1, inferior temporal gyrus; 2, middle temporal gyrus; 3, superior temporal gyrus; 4, lingual gyrus; 5, calcarine sulcus; 6, cuneus; 7, inferior occipital gyrus; 8, middle occipital gyrus; 9, superior occipital gyrus; 10, angular gyrus; 11, inferior parietal lobule; 12, supramarginal gyrus; 13, superior parietal lobule; 14, paracentral lobule; 15, somatosensory cortex; 16, primary motor cortex; 17, dorsal premotor cortex; 18, ventral premotor cortex; 19, pre-supplementary motor area; 20, supplementary motor area; 21, inferior frontal gyrus pars opercularis; 22, medial frontal gyrus; 23, middle frontal gyrus; 24, inferior frontal gyrus pars triangularis; 25, inferior frontal gyrus pars orbitalis; 26, lateral orbital gyrus; 27, superior frontal gyrus; 28, anterior orbital gyrus; 29, gyrus rectus; 30, medial orbital gyrus; 31, medial orbitofrontal gyrus; 32, olfactory cortex. All subjects in the AD cohort were obtained from the ADNI database.

frontal gyrus were located in a ventro-lateral portion of the anterior corpus callosum. While this prior study is an important advance, the current study provides a more specific topography of the anterior corpus callosum, including 12 prefrontal tracts. Further, tracts which are well-known to be in the anterior portion of the corpus callosum, including supplementary motor area, pre-supplementary motor area, dorsal premotor cortex, and premotor cortex were also evaluated. We found that the four aforementioned tracts crossed over to the posterior corpus callosum, adding to a growing body of literature demonstrating that previous segmentations of the corpus callosum can be further refined (Hofer and Frahm, 2006; Pannek et al., 2010). The use of the TCATT will allow for more specific assessments of structural deficits and structure-function relationships, as well as more enhanced measurements of disease progression, evaluation of treatment effects, and improve patient selection for clinical trials.

Principal evidence for the degeneration of the corpus callosum and the transcallosal white matter tracts in AD has been extensively explored using diffusion MRI over the last two decades; however, findings between studies have been inconsistent. For example, recent studies using a single tensor model have found reductions in fractional anisotropy (FA) in the genu of the corpus callosum (Ouyang et al., 2015), but many studies have shown no alterations in FA in the genu (Choi et al., 2005; Duan et al., 2006; Head et al., 2004; Naggara et al., 2006; Takahashi et al., 2002; Zhang et al., 2007). Similar inconsistencies have been shown in the splenium (Choi et al., 2005; Duan et al., 2006; Head et al., 2004; Naggara et al., 2006; Ouyang et al., 2015; Takahashi et al., 2002; Teipel et al., 2007; Zhang et al., 2007). It's possible that our knowledge of transcallosal degeneration in AD has been limited by three major issues. First, many studies use region-based analyses which rely on the manual delineation of certain segments of the corpus callosum. Second, many studies use FA although it is now well-known that this variable is susceptible to partial volume effects. Third, there have been no comprehensive studies of the transcallosal white matter tracts. In the current study, we used an automated approach with novel diffusion MRI metrics to comprehensively study transcallosal tract degeneration in an AD cohort dataset from the Alzheimer's Disease Neuroimaging Initiative (ADNI), and addressed the partial volume limitation of FA by performing FW correction to diffusion MRI maps–this allowed us to evaluate FW (the fluid component) and FA_T (the tissue component), separately. The assessment of FA_T and FW in the TCATT revealed robust between-group differences in FW in the absence of between-group differences in FA_T. Our findings support the idea of widespread commissural neurodegeneration in AD, and advance the field by showing this is predominantly a result of increased FW, which could be indicative of neuroinflammation or atrophy within the commissural white matter (Pasternak et al., 2009, 2012). The lack of between-group differences in FA_T could indicate that although there is increased fluid at the voxel-level (i.e., increased FW) in AD, the tissue which remains is intact (i.e., unaltered FA_T). A further strength of the current study is that tract-wide differences were followed by slice-level analysis to determine which regions of the TCATT tracts were significantly different between groups (see Supplementary Table I). T-tests corrected for multiple comparisons allowed us to determine which slices within each tract were robustly different between groups, and these significant slices were then averaged and used as independent variables in a stepwise regression analysis to determine which tracts best predicted cognitive function in the AD cohort. We found that although there were significant and widespread between-group differences in FW, the variable which most contributed to cognitive function was FW within the inferior temporal

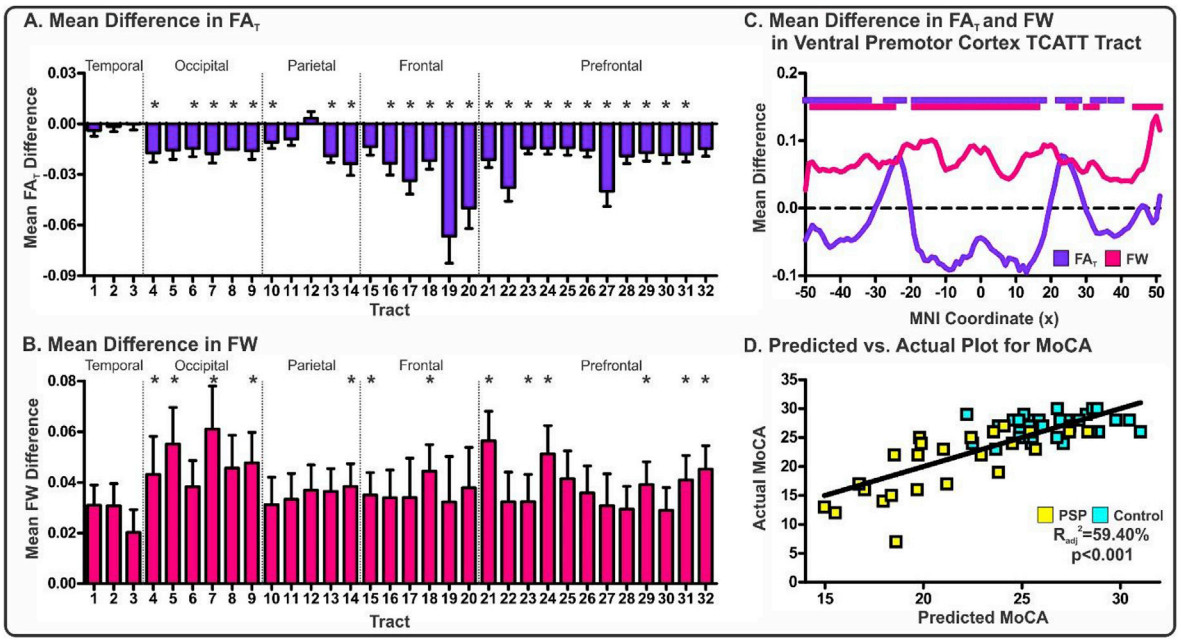

Fig. 8. Evaluation of FA_T and FW within the TCATT for the PSP Cohort. Mean differences in FA_T (**A**) and FW (**B**) for PSP-control for each TCATT tract grouped by their cortical projection (Temporal, Occipital, Parietal, Frontal, Prefrontal). Columns represent mean difference between group and error bars represent standard deviation. Significant mean differences were followed with slice-level analyses. The FA_T (blue) and FW (pink) profiles for the ventral premotor cortex TCATT tract are shown in (**C**), where FDR corrected t-tests were performed at each slice, in which age and sex were inputted as covariates. Slices which exhibited FDR corrected significance ($p_{FDR}<0.05$) are shown with horizontal blue or pink lines. (**D**) The predicted versus actual plot for the input variables which were most associated with MoCA in the PSP cohort (PSP: yellow; Control: cyan), which included gender, FA_T in the inferior frontal pars triangularis, preSMA, and medial frontal gyrus TCATT tracts as well as and FW in the inferior frontal pars opercularis TCATT tract. Abbreviations: 1, inferior temporal gyrus; 2, middle temporal gyrus; 3, superior temporal gyrus; 4, lingual gyrus; 5, calcarine sulcus; 6, cuneus; 7, inferior occipital gyrus; 8, middle occipital gyrus; 9, superior occipital gyrus; 10, angular gyrus; 11, inferior parietal lobule; 12, supramarginal gyrus; 13, superior parietal lobule; 14, paracentral lobule; 15, somatosensory cortex; 16, primary motor cortex; 17, dorsal premotor cortex; 18, ventral premotor cortex; 19, pre-supplementary motor area; 20, supplementary motor area; 21, inferior frontal gyrus pars opercularis; 22, medial frontal gyrus; 23, middle frontal gyrus; 24, inferior frontal gyrus pars triangularis; 25, inferior frontal gyrus pars orbitalis; 26, lateral orbital gyrus; 27, superior frontal gyrus; 28, anterior orbital gyrus; 29, gyrus rectus; 30, medial orbital gyrus; 31, medial orbitofrontal gyrus; 32, olfactory cortex. All subjects in the PSP cohort were obtained from the University of Florida.

gyrus TCATT tract ($R^2_{adj} = 46.975\%$, $p < 0.001$), which agrees with the idea that the inferior temporal lobe is one of the first affected regions of the brain in AD and may therefore manifest in white matter atrophy in this analysis (Braak and Braak, 1991). This finding adds to the literature by showing that FW is robustly associated with cognitive function in AD.

Studies in PSP have also been impaired by a lack of a spatially precise transcallosal tract template; thus, most studies of PSP have focused solely on region-based analyses of the corpus callosum. Structural alterations in PSP have consistently found FA reductions in the genu of the corpus callosum (Ito et al., 2008; Lehericy et al., 2010; Planetta et al., 2016; Whitwell et al., 2011). However, our application of the TCATT to a PSP cohort from the University of Florida found widespread reductions in FA_T and increases in FW. Although there were widespread differences throughout the TCATT, there were no significant between-group differences in temporal TCATT tracts, mirroring pathological findings of frontal lobe atrophy in PSP (Dickson, 2012). The slice-level analysis and stepwise regression analysis showed that FA_T in the inferior frontal pars triangularis, preSMA, and medial frontal gyrus TCATT tracts (and FW in the inferior frontal pars opercularis TCATT tract) best predicted cognitive decline ($R^2_{adj} = 59.40\%$, $p < 0.001$).

Neuroimaging is a key tool for diagnosing different neurodegenerative dementias, such as AD and PSP, as well as analyzing brain changes over time, with great interest in the earliest detectable changes. This study provides the first evidence that transcallosal FW imaging could be a potential biomarker as well as a tool that could be applied to the longitudinal progression of dementia. With the increasing value of PET approaches (Ishii, 2014) in dementia, it's possible that the TCATT could be used both to differentiate dementia subtypes and track pathway changes over time. Future studies may use this approach with the available template to determine whether therapeutic interventions are having the expected effect on brain microstructure.

A well-known limitation of diffusion MRI and tractography is the ability to model crossing fibers, particularly in areas of the brain where these are highly prevalent, such as the centrum semiovale (Wedeen et al., 2008). This limitation is lessened by using high-resolution Human Connectome Project data, which allows for the modelling of up to 3 crossing fibers per voxel. Future studies conducting tractography analysis could incorporate recent advancements, such as multi-shell multi-tissue constrained spherical deconvolution (MSMT-CST), to more successfully construct tracts (Dell'Acqua and Tournier, 2019; Maier-Hein et al., 2017). Another limitation of this study is that diffusion MRI is susceptible to partial volume effects, and therefore, measures such as fractional anisotropy can be influenced by multiple factors (e.g., axonal ordering, myelination, axonal density, gliosis) (Jones et al., 2013). In this study, we conducted a two-compartment model to split each voxel into a tissue and fluid compartment, which ameliorates the partial volumes effects due to extracellular fluid (Pasternak et al., 2009); however, future studies that acquire multi-shell diffusion MRI scans will be able to split voxels into even more compartments, such as neurite orientation dispersion and density imaging (NODDI) (Zhang et al., 2012).

5. Conclusions

This study has provided a high-resolution transcallosal tract template (TCATT) freely available at www.lrnlab.org. While the TCATT was created with the intention to investigate neurodegeneration in dementia (e.g., AD and PSP), it can also be used across a broad range of neurological and psychiatric conditions.

Funding

This work was supported by the Parkinson's Foundation (PF-FBS-1778) and National Institutes of Health (R01 NS058487, R01 NS075012, P50 AG047266, and T32 NS082168).

Acknowledgements

Data were provided [in part] by the Human Connectome Project, WU-Minn Consortium (Principal Investigators: David Van Essen and Kamil Ugurbil; 1U54MH091657) funded by the 16 NIH Institutes and Centers that support the NIH Blueprint for Neuroscience Research; and by the McDonnell Center for Systems Neuroscience at Washington University. MRI data collection for the progressive supranuclear palsy cohort was supported through the National High Magnetic Field Laboratory and obtained at the Advanced Magnetic Resonance Imaging and Spectroscopy facility in the McKnight Brain Institute of the University of Florida. MRI data for the Alzheimer's disease cohort obtained from the Alzheimer's Disease Neuroimaging Initiative database (adni.loni.usc.edu). As such, the investigators within the ADNI contributed to the design and implementation of ADNI and/or provided data but did not participate in analysis or writing of this report. A complete listing of ADNI investigators can be found at: http://adni.loni.usc.edu/wp-content/uploads/how_to_apply/ADNI_Acknowledgement_List.pdf.

Appendix A. Supplementary data

Supplementary data to this article can be found online at https://doi.org/10.1016/j.neuroimage.2019.06.065.

References

Abe, O., Masutani, Y., Aoki, S., Yamasue, H., Yamada, H., Kasai, K., Mori, H., Hayashi, N., Masumoto, T., Ohtomo, K., 2004. Topography of the human corpus callosum using diffusion tensor tractography. J. Comput. Assist. Tomogr. 28, 533–539.

Andersson, J.L.R., Sotiropoulos, S.N., 2016. An integrated approach to correction for off-resonance effects and subject movement in diffusion MR imaging. Neuroimage 125, 1063–1078.

Archer, D.B., Coombes, S.A., Chu, W.T., Chung, J.W., Burciu, R.G., Okun, M.S., Wagle Shukla, A., Vaillancourt, D.E., 2018a. A widespread visually-sensitive functional network relates to symptoms in essential tremor. Brain 141, 472–485.

Archer, D.B., Vaillancourt, D.E., Coombes, S.A., 2018b. A template and probabilistic atlas of the human sensorimotor tracts using diffusion MRI. Cerebr. Cortex 28, 1685–1699.

Arnone, D., Barrick, T.R., Chengappa, S., Mackay, C.E., Clark, C.A., Abou-Saleh, M.T., 2008. Corpus callosum damage in heavy marijuana use: preliminary evidence from diffusion tensor tractography and tract-based spatial statistics. Neuroimage 41, 1067–1074.

Avants, B.B., Epstein, C.L., Grossman, M., Gee, J.C., 2008. Symmetric diffeomorphic image registration with cross-correlation: evaluating automated labeling of elderly and neurodegenerative brain. Med. Image Anal. 12, 26–41.

Behrens, T.E., Berg, H.J., Jbabdi, S., Rushworth, M.F., Woolrich, M.W., 2007. Probabilistic diffusion tractography with multiple fibre orientations: what can we gain? Neuroimage 34, 144–155.

Behrens, T.E., Woolrich, M.W., Jenkinson, M., Johansen-Berg, H., Nunes, R.G., Clare, S., Matthews, P.M., Brady, J.M., Smith, S.M., 2003. Characterization and propagation of uncertainty in diffusion-weighted MR imaging. Magn. Reson. Med. 50, 1077–1088.

Braak, H., Braak, E., 1991. Neuropathological stageing of Alzheimer-related changes. Acta Neuropathol. 82, 239–259.

Caeyenberghs, K., Leemans, A., Coxon, J., Leunissen, I., Drijkoningen, D., Geurts, M., Gooijers, J., Michiels, K., Sunaert, S., Swinnen, S.P., 2011. Bimanual coordination and corpus callosum microstructure in young adults with traumatic brain injury: a diffusion tensor imaging study. J. Neurotrauma 28, 897–913.

Choi, S.J., Lim, K.O., Monteiro, I., Reisberg, B., 2005. Diffusion tensor imaging of frontal white matter microstructure in early Alzheimer's disease: a preliminary study. J. Geriatr. Psychiatry Neurol. 18, 12–19.

De Benedictis, A., Petit, L., Descoteaux, M., Marras, C.E., Barbareschi, M., Corsini, F., Dallabona, M., Chioffi, F., Sarubbo, S., 2016. New insights in the homotopic and heterotopic connectivity of the frontal portion of the human corpus callosum revealed by microdissection and diffusion tractography. Hum. Brain Mapp. 37, 4718–4735.

Dell'Acqua, F., Tournier, J.D., 2019. Modelling white matter with spherical deconvolution: how and why? NMR Biomed. 32, e3945.

Desikan, R.S., Segonne, F., Fischl, B., Quinn, B.T., Dickerson, B.C., Blacker, D., Buckner, R.L., Dale, A.M., Maguire, R.P., Hyman, B.T., Albert, M.S., Killiany, R.J., 2006. An automated labeling system for subdividing the human cerebral cortex on MRI scans into gyral based regions of interest. Neuroimage 31, 968–980.

Dickson, D.W., 2012. Parkinson's disease and parkinsonism: neuropathology. Cold Spring Harb Perspect Med 2.

Duan, J.H., Wang, H.Q., Xu, J., Lin, X., Chen, S.Q., Kang, Z., Yao, Z.B., 2006. White matter damage of patients with Alzheimer's disease correlated with the decreased cognitive function. Surg. Radiol. Anat. 28, 150–156.

Feinberg, D.A., Moeller, S., Smith, S.M., Auerbach, E., Ramanna, S., Gunther, M., Glasser, M.F., Miller, K.L., Ugurbil, K., Yacoub, E., 2010. Multiplexed echo planar imaging for sub-second whole brain FMRI and fast diffusion imaging. PLoS One 5 e15710.

Fling, B.W., Benson, B.L., Seidler, R.D., 2013. Transcallosal sensorimotor fiber tract structure-function relationships. Hum. Brain Mapp. 34, 384–395.

Head, D., Buckner, R.L., Shimony, J.S., Williams, L.E., Akbudak, E., Conturo, T.E., McAvoy, M., Morris, J.C., Snyder, A.Z., 2004. Differential vulnerability of anterior white matter in nondemented aging with minimal acceleration in dementia of the Alzheimer type: evidence from diffusion tensor imaging. Cerebr. Cortex 14, 410–423.

Hofer, S., Frahm, J., 2006. Topography of the human corpus callosum revisited–comprehensive fiber tractography using diffusion tensor magnetic resonance imaging. Neuroimage 32, 989–994.

Huang, H., Zhang, J., Jiang, H., Wakana, S., Poetscher, L., Miller, M.I., van Zijl, P.C., Hillis, A.E., Wytik, R., Mori, S., 2005. DTI tractography based parcellation of white matter: application to the mid-sagittal morphology of corpus callosum. Neuroimage 26, 195–205.

Ishii, K., 2014. PET approaches for diagnosis of dementia. AJNR Am J Neuroradiol 35, 2030–2038.

Ito, S., Makino, T., Shirai, W., Hattori, T., 2008. Diffusion tensor analysis of corpus callosum in progressive supranuclear palsy. Neuroradiology 50, 981–985.

Jack Jr., C.R., Bennett, D.A., Blennow, K., Carrillo, M.C., Dunn, B., Haeberlein, S.B., Holtzman, D.M., Jagust, W., Jessen, F., Karlawish, J., Liu, E., Molinuevo, J.L., Montine, T., Phelps, C., Rankin, K.P., Rowe, C.C., Scheltens, P., Siemers, E., Snyder, H.M., Sperling, R., Contributors, 2018. NIA-AA Research Framework: toward a biological definition of Alzheimer's disease. Alzheimers Dement 14, 535–562.

Jenkinson, M., Beckmann, C.F., Behrens, T.E., Woolrich, M.W., Smith, S.M., 2012. Fsl. Neuroimage 62, 782–790.

Jones, D.K., Knosche, T.R., Turner, R., 2013. White matter integrity, fiber count, and other fallacies: the do's and don'ts of diffusion MRI. Neuroimage 73, 239–254.

Lebel, C., Caverhill-Godkewitsch, S., Beaulieu, C., 2010. Age-related regional variations of the corpus callosum identified by diffusion tensor tractography. Neuroimage 52, 20–31.

Lehericy, S., Hartmann, A., Lannuzel, A., Galanaud, D., Delmaire, C., Bienaimee, M.J., Jodoin, N., Roze, E., Gaymard, B., Vidailhet, M., 2010. Magnetic resonance imaging lesion pattern in Guadeloupean parkinsonism is distinct from progressive supranuclear palsy. Brain 133, 2410–2425.

Liu, I.C., Chiu, C.H., Chen, C.J., Kuo, L.W., Lo, Y.C., Tseng, W.Y., 2010. The microstructural integrity of the corpus callosum and associated impulsivity in alcohol dependence: a tractography-based segmentation study using diffusion spectrum imaging. Psychiatr. Res. 184, 128–134.

Maier-Hein, K.H., Neher, P.F., Houde, J.C., Cote, M.A., Garyfallidis, E., Zhong, J., Chamberland, M., Yeh, F.C., Lin, Y.C., Ji, Q., Reddick, W.E., Glass, J.O., Chen, D.Q., Feng, Y., Gao, C., Wu, Y., Ma, J., Renjie, H., Li, Q., Westin, C.F., Deslauriers-Gauthier, S., Gonzalez, J.O.O., Paquette, M., St-Jean, S., Girard, G., Rheault, F., Sidhu, J., Tax, C.M.W., Guo, F., Mesri, H.Y., David, S., Froeling, M., Heemskerk, A.M., Leemans, A., Bore, A., Pinsard, B., Bedetti, C., Desrosiers, M., Brambati, S., Doyon, J., Sarica, A., Vasta, R., Cerasa, A., Quattrone, A., Yeatman, J., Khan, A.R., Hodges, W., Alexander, S., Romascano, D., Barakovic, M., Auria, A., Esteban, O., Lemkaddem, A., Thiran, J.P., Cetingul, H.E., Odry, B.L., Mailhe, B., Nadar, M.S., Pizzagalli, F., Prasad, G., Villalon-Reina, J.E., Galvis, J., Thompson, P.M., Requejo, F.S., Laguna, P.L., Lacerda, L.M., Barrett, R., Dell'Acqua, F., Catani, M., Petit, L., Caruyer, E., Daducci, A., Dyrby, T.B., Holland-Letz, T., Hilgetag, C.C., Stieltjes, B., Descoteaux, M., 2017. The challenge of mapping the human connectome based on diffusion tractography. Nat. Commun. 8, 1349.

Mayka, M.A., Corcos, D.M., Leurgans, S.E., Vaillancourt, D.E., 2006. Three-dimensional locations and boundaries of motor and premotor cortices as defined by functional brain imaging: a meta-analysis. Neuroimage 31, 1453–1474.

Moeller, S., Yacoub, E., Olman, C.A., Auerbach, E., Strupp, J., Harel, N., Ugurbil, K., 2010. Multiband multislice GE-EPI at 7 tesla, with 16-fold acceleration using partial parallel imaging with application to high spatial and temporal whole-brain fMRI. Magn. Reson. Med. 63, 1144–1153.

Naggara, O., Oppenheim, C., Rieu, D., Raoux, N., Rodrigo, S., Dalla Barba, G., Meder, J.F., 2006. Diffusion tensor imaging in early Alzheimer's disease. Psychiatr. Res. 146, 243–249.

Nasreddine, Z.S., Phillips, N.A., Bedirian, V., Charbonneau, S., Whitehead, V., Collin, I., Cummings, J.L., Chertkow, H., 2005. The Montreal Cognitive Assessment, MoCA: a brief screening tool for mild cognitive impairment. J. Am. Geriatr. Soc. 53, 695–699.

Ofori, E., Pasternak, O., Planetta, P.J., Burciu, R., Snyder, A., Febo, M., Golde, T.E., Okun, M.S., Vaillancourt, D.E., 2015. Increased free water in the substantia nigra of Parkinson's disease: a single-site and multi-site study. Neurobiol. Aging 36, 1097–1104.

Ouyang, X., Chen, K., Yao, L., Hu, B., Wu, X., Ye, Q., Guo, X., Alzheimer's Disease Neuroimaging, I., 2015. Simultaneous changes in gray matter volume and white matter fractional anisotropy in Alzheimer's disease revealed by multimodal CCA and joint ICA. Neuroscience 301, 553–562.

Pannek, K., Mathias, J.L., Bigler, E.D., Brown, G., Taylor, J.D., Rose, S., 2010. An automated strategy for the delineation and parcellation of commissural pathways suitable for clinical populations utilising high angular resolution diffusion imaging tractography. Neuroimage 50, 1044–1053.

Pasternak, O., Sochen, N., Gur, Y., Intrator, N., Assaf, Y., 2009. Free water elimination and mapping from diffusion MRI. Magn. Reson. Med. 62, 717–730.

Pasternak, O., Westin, C.F., Bouix, S., Seidman, L.J., Goldstein, J.M., Woo, T.U., Petryshen, T.L., Mesholam-Gately, R.I., McCarley, R.W., Kikinis, R., Shenton, M.E., Kubicki, M., 2012. Excessive extracellular volume reveals a neurodegenerative pattern in schizophrenia onset. J. Neurosci. 32, 17365–17372.

Planetta, P.J., Ofori, E., Pasternak, O., Burciu, R.G., Shukla, P., DeSimone, J.C., Okun, M.S., McFarland, N.R., Vaillancourt, D.E., 2016. Free-water imaging in Parkinson's disease and atypical parkinsonism. Brain 139, 495–508.

Setsompop, K., Gagoski, B.A., Polimeni, J.R., Witzel, T., Wedeen, V.J., Wald, L.L., 2012. Blipped-controlled aliasing in parallel imaging for simultaneous multislice echo planar imaging with reduced g-factor penalty. Magn. Reson. Med. 67, 1210–1224.

Smith, S.M., 2002. Fast robust automated brain extraction. Hum. Brain Mapp. 17, 143–155.

Smith, S.M., Jenkinson, M., Woolrich, M.W., Beckmann, C.F., Behrens, T.E., Johansen-Berg, H., Bannister, P.R., De Luca, M., Drobnjak, I., Flitney, D.E., Niazy, R.K., Saunders, J., Vickers, J., Zhang, Y., De Stefano, N., Brady, J.M., Matthews, P.M., 2004. Advances in functional and structural MR image analysis and implementation as FSL. Neuroimage 23 (Suppl. 1), S208–S219.

Sotiropoulos, S.N., Jbabdi, S., Xu, J., Andersson, J.L., Moeller, S., Auerbach, E.J., Glasser, M.F., Hernandez, M., Sapiro, G., Jenkinson, M., Feinberg, D.A., Yacoub, E., Lenglet, C., Van Essen, D.C., Ugurbil, K., Behrens, T.E., 2013a. Advances in diffusion MRI acquisition and processing in the human connectome Project. Neuroimage 80, 125–143.

Sotiropoulos, S.N., Moeller, S., Jbabdi, S., Xu, J., Andersson, J.L., Auerbach, E.J., Yacoub, E., Feinberg, D., Setsompop, K., Wald, L.L., Behrens, T.E., Ugurbil, K., Lenglet, C., 2013b. Effects of image reconstruction on fiber orientation mapping from multichannel diffusion MRI: reducing the noise floor using SENSE. Magn. Reson. Med. 70, 1682–1689.

Takahashi, S., Yonezawa, H., Takahashi, J., Kudo, M., Inoue, T., Tohgi, H., 2002. Selective reduction of diffusion anisotropy in white matter of Alzheimer disease brains measured by 3.0 Tesla magnetic resonance imaging. Neurosci. Lett. 332, 45–48.

Teipel, S.J., Stahl, R., Dietrich, O., Schoenberg, S.O., Perneczky, R., Bokde, A.L., Reiser, M.F., Moller, H.J., Hampel, H., 2007. Multivariate network analysis of fiber tract integrity in Alzheimer's disease. Neuroimage 34, 985–995.

Tomasch, J., 1954. Size, distribution, and number of fibres in the human corpus callosum. Anat. Rec. 119, 119–135.

Tzourio-Mazoyer, N., Landeau, B., Papathanassiou, D., Crivello, F., Etard, O., Delcroix, N., Mazoyer, B., Joliot, M., 2002. Automated anatomical labeling of activations in SPM using a macroscopic anatomical parcellation of the MNI MRI single-subject brain. Neuroimage 15, 273–289.

Van Essen, D.C., Smith, S.M., Barch, D.M., Behrens, T.E., Yacoub, E., Ugurbil, K., 2013. The Wu-minn human connectome Project: an overview. Neuroimage 80, 62–79.

Wedeen, V.J., Wang, R.P., Schmahmann, J.D., Benner, T., Tseng, W.Y., Dai, G., Pandya, D.N., Hagmann, P., D'Arceuil, H., de Crespigny, A.J., 2008. Diffusion spectrum magnetic resonance imaging (DSI) tractography of crossing fibers. Neuroimage 41, 1267–1277.

Whitwell, J.L., Master, A.V., Avula, R., Kantarci, K., Eggers, S.D., Edmonson, H.A., Jack Jr., C.R., Josephs, K.A., 2011. Clinical correlates of white matter tract degeneration in progressive supranuclear palsy. Arch. Neurol. 68, 753–760.

Woolrich, M.W., Jbabdi, S., Patenaude, B., Chappell, M., Makni, S., Behrens, T., Beckmann, C., Jenkinson, M., Smith, S.M., 2009. Bayesian analysis of neuroimaging data in FSL. Neuroimage 45, S173–S186.

Zhang, H., Schneider, T., Wheeler-Kingshott, C.A., Alexander, D.C., 2012. NODDI: practical in vivo neurite orientation dispersion and density imaging of the human brain. Neuroimage 61, 1000–1016.

Zhang, Y., Schuff, N., Jahng, G.H., Bayne, W., Mori, S., Schad, L., Mueller, S., Du, A.T., Kramer, J.H., Yaffe, K., Chui, H., Jagust, W.J., Miller, B.L., Weiner, M.W., 2007. Diffusion tensor imaging of cingulum fibers in mild cognitive impairment and Alzheimer disease. Neurology 68, 13–19.